ELSEVIER

International Journal of Heat and Fluid Flow 19 (1998) 297–306

International Journal of HEAT AND FLUID FLOW

Non-linear eddy-viscosity modelling of transitional boundary layers pertinent to turbomachine aerodynamics

W.L. Chen, F.S. Lien, M.A. Leschziner *

Department of Mechanical Engineering, Institute of Science and Technology, University of Manchester, P.O. Box 88, Manchester M60 1QD, UK

Received 14 January 1997; accepted 24 September 1997

Abstract

The predictive performance of three low-Reynolds-number turbulence models, one based on the linear (Boussinesq) stress-strain relationship and two adopting cubic forms, is examined by reference to transitional flat-plate boundary layers subjected to streamwise pressure gradient and moderate free-stream turbulence, the latter causing bypass transition. One of the cubic models involves the solution of two transport equations, while the other involves three equations, one of which relates to the second invariant of turbulence anisotropy. The investigation demonstrates that, for the conditions examined, the non-linear models return a more credible representation of transition than the linear variant, although none of the models may be said to be entirely satisfactory. Thus, while non-linear modelling shows promise and offers inherent advantages through the use of a more general stress-strain linkage and elaborate calibration, further refinement is needed in the present cubic variants for transitional flows.

Keywords: Turbulence; Non-linear eddy-viscosity models; Bypass transition; Turbomachinery

Notation

A	Lumley's flatness parameter ($\equiv 1-\frac{9}{8}(A_2-A_3)$)
A^*, A', A''	effective values of A
A_2	second invariant of the Reynolds stress anisotropy ($\equiv a_{ij}a_{ij}$)
A_3	third invariant of the Reynolds stress anisotropy ($\equiv a_{ik}a_{kj}a_{ji}$)
a_{ij}	stress anisotropy ($\equiv \overline{u_i'u_j'}/k-\frac{2}{3}\delta_{ij}$)
C_f	skin-friction coefficient
c_1–c_5	coefficients in the cubic stress-strain/vorticity relation
$c_{\varepsilon 1}, c_{\varepsilon 2}$	coefficients in ε-equation
c_μ	coefficient in eddy-viscosity relation
f_μ	damping coefficient in low-Reynolds-number turbulence models
K	acceleration parameter ($\equiv (\nu/u_\infty)\,\mathrm{d}u_\infty/\mathrm{d}x$)
k	turbulence energy
l_ε	free-stream dissipation-length scale ($\equiv k^{1.5}/\varepsilon$)
P_k	production of turbulence energy k
$\mathrm{Re}_x, \mathrm{Re}_\theta$	Reynolds numbers based on streamwise length and momentum-thickness, respectively
$\tilde{R}_t$	local turbulence Reynolds number ($\equiv k^2/\nu\tilde{\varepsilon}$)
S_{ij}	strain tensor ($\equiv \partial u_i/\partial x_j+\partial u_j/\partial x_i$)
$S, \tilde{S}$	strain invariants ($\equiv k/\varepsilon\sqrt{S_{ij}S_{ij}/2}, k/\tilde{\varepsilon}\sqrt{S_{ij}S_{ij}/2}$, respectively)
Tu	turbulence intensity
$u_{i,i=1,2}$	mean-velocity component in the x_i-direction
u', v', w'	turbulence intensity in the x, y and z directions, respectively
$\overline{u_i'u_j'}$	Reynolds-stress tensor
$x_{i,i=1,2}$	Cartesian coordinates
y^+	universal wall distance ($\equiv yu_\tau/\nu$)

Greek

γ	intermittency
θ	momentum thickness
λ_θ	pressure gradient parameter ($\equiv(\theta^2/\nu)\,\mathrm{d}u/\mathrm{d}x$)
δ_{ij}	Kronecker delta
ε	dissipation rate of k
$\tilde{\varepsilon}$	isotropic dissipation rate of k
μ_t	turbulent viscosity
ν	kinematic fluid viscosity
ν_t	μ_t/ρ
Ω_{ij}	vorticity tensor ($\equiv \partial u_i/\partial x_j-\partial u_j/\partial x_i$)
$\Omega, \tilde{\Omega}$	vorticity invariants ($\equiv k/\varepsilon\sqrt{\Omega_{ij}\Omega_{ij}/2}, k/\tilde{\varepsilon}\sqrt{\Omega_{ij}\Omega_{ij}/2}$, respectively)
ρ	fluid density

1. Introduction

Although the flow in the blade passages of a typical multistage turbomachine is highly turbulent, the Reynolds number based on the blade chord is often quite low (of the order 1×10^6 or less), even in large gas turbines. Moreover, substantial portions of the flow around the blades of both turbine and

* Corresponding author. E-mail: m.leschziner@umist.ac.uk.

0142-727X/98/$19.00
PII: S0142-727X(97)10012-1

compressor stages are subjected to acceleration. The above two facts combine to render boundary-layer transition a process which can have a substantial influence on the operational characteristics of gas-turbine engines.

In compressors, the bulk relative flow is decelerating, and transition tends to be completed relatively quickly. In contrast, the bulk relative flow in a turbine is accelerating, and transition is both delayed and prolonged in terms of its spatial extent. No matter how transition evolves, the process leads to a dramatic rise in skin friction, boundary-layer thickness and heat transfer, all important in relation to the evolution of the boundary layers on the blade downstream of the transition point and hence to the blade's operational performance. Therefore, the study and description of transition contribute greatly to the objective of correctly predicting turbomachinery flows.

Transition may be divided into three different basic modes: the *natural*, the *by-pass* and the *separated-flow* mode. Mayle (1991) has given the most comprehensive overview to date of the role of laminar-to-turbulent transition in gas-turbine engines. This review attempts to provide a unified approach to the whole range of transition phenomena encountered in compressors and turbines, and it offers a means of specifying transition empirically within computational approaches which are inherently incapable of capturing the associated physical processes. Mayle's considerations are based on the description of transition by Emmons (1951). This defines the fraction of time during which the flow at any point in the boundary layer is turbulent as the "intermittency" γ, with $\gamma = 0$ denoting laminar flow, $\gamma = 1$ denoting turbulent flow, and $0 < \gamma < 1$ identifying the transitional state. Emmons further assumes that the time-averaged flow at any streamwise position can be regarded as a superposition of laminar- and turbulent-flow components, and the transition process is determined by the onset-of-transition Reynolds number, Re_{xt}, and the spot-production parameter via appropriate flow parameters affecting them. These parameters were noted by Abu-Ghannam and Shaw (1980) to include the free-stream turbulence intensity, the pressure gradient, the Reynolds number, the Mach number, acoustic radiation, surface roughness, surface temperature, surface curvature, heat transfer and the history of the processes associated with some of these parameters. Mayle (1991) has stated that the first three are the most influential, and has thus correlated the onset-of-transition Reynolds number and spot-production parameter with the free-stream turbulence intensity Tu and the pressure gradient, using available experimental data. To account for the effect of pressure gradient, the related parameter $\lambda_\theta = (\theta^2/\nu)\mathrm{d}u_\infty/\mathrm{d}x$ or the acceleration parameter $K = (\nu/u_\infty)\mathrm{d}u_\infty/\mathrm{d}x$ at transition are commonly used. With reference to the data of Blair (1983), Mayle has argued that K is more appropriate for flows subjected to favourable pressure gradient, where transition is principally of the by-pass type, and it is this parameter he has chosen for his correlations. However, Mayle's correlations only apply to specific upstream conditions, and variations in these cannot be taken into account. In flows over compressor or turbine blades, the pressure gradient varies greatly along the blade surface so that the exclusion of variations in upstream pressure gradient and turbulence conditions is unreasonable. Besides, most of the studies reviewed focus on simple geometries, rather than on the kind of complex conditions encountered in turbomachinery flows. Hence, the extent to which Mayle's correlations are applicable in real blade flows is not clear.

Rather than using simple empirical correlations of the above type to solve complex transitional turbomachinery flows, an alternative route offering the promise of broader applicability and improved realism is one in which the full Reynolds-averaged Navier–Stokes equations are solved with a high-quality turbulence model that describes non-equilibrium processes. While the process of bypass transition appears to be influenced materially by the propagation of pressure fluctuations from the free stream into the boundary layer and also seems preferentially sensitive to wall-normal turbulence fluctuations, relative to other components (Yang et al., 1994), the expectation is that any model accounting for the diffusive transport of turbulence from the free stream into the boundary layer will have the potential of capturing the essential phenomenological features of transition. Indeed, it is this expectation which underpins intensive, ongoing efforts to investigate the performance of conventional statistical closures for low-Re transitional flows.

To examine and quantify the ability of different models to simulate transition, an ERCOFTAC-led international initiative was launched in 1991 (Savill, 1991). A wide range of test cases – some highly idealised, others close to real conditions and all carefully measured – had been selected for investigation. Among them, two cases – "T3A" and "T3B" – focus on transition in a flat-plate boundary layer with zero-pressure gradient. A group of other cases – all denoted by "T3C" – is concerned with transition in flat-plate boundary layers subjected to various pressure gradients. A fourth type of flow – that developing over a flat plate with a semi-circular leading edge and denoted by "T3L" – has also been included in an effort to understand the process of transition in the flow around the rounded leading edge of a blade and to quantify the ability of turbulence models to resolve the process of separation-induced transition. The above test cases form a comprehensive framework within which fundamental transitional phenomena of the type encountered in turbomachinery flows may be studied. Many research groups have contributed computational solutions to this exercise, and almost the whole range of currently available turbulence-closure approaches have been investigated (Savill, 1995a). At the linear eddy-viscosity k–ε level of closure, results by several groups have indicated that the R_t-dependent low-Reynolds-number formulation of Launder and Sharma (1974) provides the best predictions for zero-pressure-gradient boundary layers. This success seems to arise from the fact that the model uses R_t, rather than the wall-distance, to characterize near-wall viscous effects on turbulence, and from the particular functional relationships used to sensitize the turbulent viscosity to the fluid viscosity. However, Savill (1995a) has reported that this model, as well as most other low-Reynolds-number variants excluding specific modifications, return solutions which exhibit substantial discrepancies relative to measurements in flows subjected to pressure gradients. This suggests that some mechanism needs to be incorporated into these models to sensitize them to the strain rate, especially the irrotational components. The observation that the onset of transition is particularly sensitive to the level of wall-normal stress also suggests the need for anisotropy-resolving models.

In view of the above facts, it would seem that a potentially promising route to predicting by-pass transition is to use nonlinear eddy-viscosity models. Such models resolve normal-stress anisotropy, are sensitive to curvature strain and return a substantially different response of turbulence to rotational and irrotational straining, in accord with reality. Important, from a practical point of view, is the fact that the increase in computational costs associated with this level of modelling, relative to the linear eddy-viscosity form, is only marginal. This is in contrast to approaches based on second-moment closure (e.g. Savill, 1995b) which, whilst offering the prospect of greater universality, involve significant cost penalties in complex flows. Yet another practical constraint is that the modelling principles adopted should not be specific to transitional flows and should be applicable to general geometric and flow conditions in which transition may or may not arise and in

which nothing is known about the effect of transition-related quantities on the boundary conditions. This is satisfied by the present model type, in contrast, for example, to approaches using an evolution equation for the intermittency γ (e.g. Steelant and Dick, 1994).

Attention is focused here specifically on the non-linear models of Craft et al. (1997) which are based on two and three transport equations for scalar turbulence parameters and are recommended by the originators for transitional flows. The objective of this paper is to assess the capabilities of these models, relative to the best linear variant of Launder and Sharma, when used to predict transition in boundary layers pertinent to turbomachine flows, especially those subjected to streamwise pressure gradient. In a follow-up paper (Chen et al., 1998), the performance of the same models is examined when these are applied to highly loaded compressor cascade profiles.

2. Turbulence Models

2.1. Rationale

Linear eddy-viscosity models are known to be afflicted with several important weaknesses, among them an inability to capture Reynolds-stress anisotropy, insufficient sensitivity to secondary strains and seriously excessive generation of turbulence in impingement regions. Non-linear forms, on the other hand, are designed to give improved performance through the inclusion of quadratic stress and vorticity components to capture anisotropy, and cubic products to return an appropriate sensitivity to curvature. Cubic variants for low-Re flows, one involving the solution of equations for k and ε, and the other an additional equation for the second invariant of stress anisotropy $a_{ij}a_{ij}$, have first been devised by Craft et al. (1993, 1997). An important feature of these models is that the eddy viscosity is made a function of strain and vorticity invariants through calibration by reference to DNS data for homogeneous shear flows. The function is so formulated as to effect a decrease in turbulence energy, through a reduction in the eddy-viscosity coefficient c_μ, in regions of large strain, such as in impingement regions and along curved shear layers. This modelling framework has been demonstrated to give satisfactory results in several flows, including homogeneous shear flow, fully developed pipe flow with and without rotation, fully developed curved-channel flow and an impinging jet. Indeed, its predictive accuracy has been found to be comparable to that attained with the Reynolds-stress model at only 1/3–1/5 of CPU consumption. However, a number of weaknesses have been identified in the two-equation variant. One is that an undesirably strong sensitivity to the Reynolds number is required in the "viscous damping function" f_μ pre-multiplying c_μ in order to achieve agreement with experiment. Another is that the model cannot faithfully reproduce the behaviour of the normal stresses close to the wall. Furthermore, the reliance of the model on a correction proposed by Yap (1987) in the context of linear eddy-viscosity modelling, which forces the ε-equation to give a broadly correct near-wall length-scale variation, raises the difficulty in complex geometries of requiring the evaluation of the minimum distances from computational nodes to the wall.

The above defects have motivated the inclusion into the model of a third transport equation for the second invariant of the Reynolds stresses $A_2(=a_{ij}a_{ij})$, derived from full second-moment closure. One important benefit arising from this approach is that the above stress invariant can be used much more effectively than the strain invariant S for controlling wall-induced damping of the eddy viscosity (through the damping function f_μ). This is because, as indicated by DNS data of Kim et al. (1987), the variation of the former is much more pronounced than that of the latter in the region $y^+ < 60$ in which damping is required. Associated with the above is the advantage that the three-equation form only requires a weak Reynolds-number dependence which may be limited to $y^+ < 10$. Finally, the model replaces the Yap correction by a new term which adopts gradients of the turbulent length scale in place of wall-normal distances. In terms of predictive realism, the model has been shown to return distribution of normal stresses which are in excellent agreement with DNS data in fully developed channel flow (Suga, 1995).

2.2. The cubic models – Mathematical foundation

The foundation of all cubic models is a general constituitive equation which links the Reynolds-stress tensor to all quadratic and cubic combinations of the strain and vorticity tensors and satisfies all requisite symmetry and contraction properties. Using the turbulence energy and its rate of dissipation to represent, respectively, the turbulent velocity and length scales, this equation can be written as follows,

$$\begin{aligned}\frac{\overline{u_i'u_j'}}{k} &= \frac{2}{3}\delta_{ij} - \frac{v_t}{k}S_{ij} + c_1\frac{v_t}{\tilde{\varepsilon}}\left(S_{ik}S_{kj} - \frac{1}{3}\delta_{ij}S_{kl}S_{kl}\right)\\ &\quad + c_2\frac{v_t}{\tilde{\varepsilon}}\left(\Omega_{ik}S_{kj} + \Omega_{jk}S_{ki}\right) + c_3\frac{v_t}{\tilde{\varepsilon}}\left(\Omega_{ik}\Omega_{jk} - \frac{1}{3}\delta_{ij}\Omega_{kl}\Omega_{kl}\right)\\ &\quad + c_4\frac{v_tk}{\tilde{\varepsilon}^2}\left(S_{ki}\Omega_{lj} + S_{kj}\Omega_{li}\right)S_{kl} + c_5\frac{v_tk}{\tilde{\varepsilon}^2}\left(S_{kl}S_{kl} - \Omega_{kl}\Omega_{kl}\right)S_{ij}.\end{aligned} \tag{1}$$

Different model variants arise from different approaches to determining the coefficients c_1–c_5 and from differences in the scale-determining transport equations.

In the two-equation model of Craft et al. (1993), the coefficients c_1–c_5 take the numerical values given in Table 1.

The eddy viscosity, turbulence energy and rate of homogeneous dissipation

$$\tilde{\varepsilon} = \varepsilon - 2\nu\left(\frac{\partial\sqrt{k}}{\partial x_i}\right)^2$$

are obtained, respectively, from

$$v_t = c_\mu f_\mu \frac{k^2}{\tilde{\varepsilon}}, \tag{2}$$

$$\frac{\partial u_i k}{\partial x_i} = \frac{\partial}{\partial x_i}\left[(\nu + v_t)\frac{\partial k}{\partial x_i}\right] + P_k - \varepsilon, \tag{3}$$

$$\frac{\partial u_i\tilde{\varepsilon}}{\partial x_i} = \frac{\partial}{\partial x_i}\left[\left(\nu + \frac{v_t}{1.3}\right)\frac{\partial\tilde{\varepsilon}}{\partial x_i}\right] + \frac{\tilde{\varepsilon}}{k}\left(c_{\varepsilon1}P_k - c_{\varepsilon2}\tilde{\varepsilon}\right) + E + Y, \tag{4}$$

in which c_μ, f_μ, E, $c_{\varepsilon1}$ and $c_{\varepsilon2}$ take the following values or functional forms,

$$\begin{aligned}c_\mu &= \frac{0.3\left[1 - \exp\left\{-0.36/\exp[-0.75\ \max(\tilde{S},\tilde{\Omega})]\right\}\right]}{1 + 0.35\{\max(\tilde{S},\tilde{\Omega})\}^{1.5}},\\ f_\mu &= 1 - \exp\left\{-\left(\frac{\tilde{R}_t}{90}\right)^{0.5} - \left(\frac{\tilde{R}_t}{400}\right)^2\right\},\end{aligned} \tag{5}$$

Table 1
Coefficients for the two-equation cubic eddy-viscosity model of Craft et al. (1993)

c_1	c_2	c_3	c_4	c_5
−0.1	0.1	0.26	$-10c_\mu^2$	$-5c_\mu^2$

Table 2
Coefficients for the three-equation cubic eddy-viscosity model of Craft et al. (1997)

c_1	c_2	c_3	c_4	c_5
$-0.05\ f_g$	$0.11\ f_g$	$0.21\ f_g[(2S)/(S+\Omega)]$	$-0.8\ f_c$	$0.5\ f_c$

$$E = 0.0022\frac{\tilde{S}v_t k^2}{\tilde{\varepsilon}}\left(\frac{\partial^2 u_i}{\partial x_j \partial x_k}\right)^2,$$

$$c_{\varepsilon 1} = 1.44, \quad c_{\varepsilon 2} = 1.92[1 - 0.3\ \exp(-\tilde{R}_t^2)], \tag{6}$$

and

$$Y = \max\left\{0.83\left(\frac{k^{1.5}}{2.5\tilde{\varepsilon}y} - 1\right)\left(\frac{k^{1.5}}{2.5\tilde{\varepsilon}y}\right)^2\frac{\tilde{\varepsilon}^2}{k},\ 0\right\} \tag{7}$$

is the "Yap correction" (Yap, 1987) which is designed to counteract the excessive rise in the turbulent length scale in boundary layers subjected to adverse pressure gradient.

The corresponding expressions for the three-equation model are

$$c_\mu = \frac{0.667 r_\eta}{1 + 1.8\eta}\left[1 - \exp\left\{\frac{-0.145}{\exp(-1.3\eta^{5/6})}\right\}\right],$$

$$f_\mu = \frac{1.1\sqrt{\tilde{\varepsilon}/\varepsilon}\{1 - 0.8\ \exp(-\tilde{R}_t/30)\}}{1 + 0.6A_2 + 0.2A_2^{3.5}}, \tag{8}$$

$$E = 1.2\nu v_t \frac{\partial^2 u_i}{\partial x_k \partial x_j}\frac{\partial^2 u_i}{\partial x_k \partial x_j} + \nu\frac{v_t}{k}\frac{\partial k}{\partial x_k}\frac{\partial u_i}{\partial x_l}\frac{\partial^2 u_i}{\partial x_k \partial x_l}, \tag{9}$$

$$c_{\varepsilon 1} = 1 + 0.15(1 - A^*),$$

$$c_{\varepsilon 2} = \frac{1.92}{1 + 0.7(1 - 1/1 + (\tilde{R}_t/20)^2\sqrt{A_2}\ \max(0.25, A^*)}, \tag{10}$$

and

$$Y = 0, \tag{11}$$

where r_η and η are

$$r_\eta = 1 + [1 - \exp\{-(A_2/0.5)^3\}] \times [1 + 4\sqrt{\exp(-\tilde{R}_t/20)}],$$

$$\eta = \max(\tilde{S}, \tilde{\Omega}) r_\eta. \tag{12}$$

In the above, A^* is a modified form of the "flatness factor" $A(\equiv 1 - (9/8)(A_2 - A_3)$, $A_3 = a_{ij}a_{jk}a_{ki})$ and is defined as

$$A^* = f_A A' + (1 - f_A)A'', \tag{13}$$

where

$$f_A = \exp(-20A''), \quad A' = A\left\{1 - \exp\left(\frac{-\tilde{R}_t^2}{1 + 24A_2}\right)\right\},$$

$$A'' = \{1 - \tfrac{9}{8}(A_2 - A_3(A_2/a_{ij}a_{ij}))^{1.5}\} \times [1 - \exp\{-(\tilde{R}_t/10)^2\}]\frac{\tilde{\varepsilon}}{\varepsilon}. \tag{14}$$

Note that A_2 in (13) is obtained from an associated transport equation derived from second-moment closure and given in Craft et al. (1997), while $a_{ij}a_{ij}$ is obtained algebraically from the stress field predicted by (1). Finally, the coefficients c_1–c_5 pertaining to the three-equation model are given in Table 2 in which the functions f_c and f_g are given by

$$f_g = \frac{r_\eta}{f_\mu\sqrt{1 + 0.0086\eta^2}}, \quad f_c = \frac{r_\eta^2}{1 + 0.45\eta^{2.5}} \tag{15}$$

3. Numerical approach

The computational solutions to follow have been obtained with the multi-block version of the general non-orthogonal, fully collocated finite-volume algorithm 'STREAM' (Lien and Leschziner, 1994a, b). In this, convection is represented by the quadratic 'QUICK' scheme (Leonard, 1979) or by the second-order TVD (Total Variation Diminishing) approximation, 'MUSCL' (van Leer, 1979). All transport equations are solved to at least second-order accuracy. This turns out to be especially important in transitional flows which are very sensitive to numerical errors. Solutions are iterated to convergence using a conventional pressure-correction approach.

4. Results and discussion

4.1. Flow over a flat plate with a sharp leading edge at zero pressure gradient

Among the test cases proposed in the ERCOFTAC transitional-flow project, the simplest (though fundamentally important) one is the flow over a flat-plate with a sharp leading edge at zero pressure-gradient. This simplicity facilitates a wide-ranging investigation with different models using economical numerical schemes. There are several test cases in this group, denoted by T3A, T3A$^-$, T3B, T3B$^+$ and T3B$_{DNS}$. Here, only case T3A is presented; results for T3B may be found in Chen (1996). High-quality and very detailed experimental data for this case have been obtained by Roach and Brierley (1992) in the facility shown in Fig. 1. The use of the elliptic code outlined in Section 3 allows the flow-inlet boundary to be placed well upstream of the leading-edge. Although this might appear rather extravagant in terms of resource requirements, an important advantage is that the calculated results are free from errors arising from the prescription of the initial profiles. Thus, this approach requires only the specification of the uniform velocity at the upstream plane and of the free-stream turbulence quantities given by

$$k_0 = 1.5(\mathrm{Tu}\ u_0)^2, \quad \varepsilon_0 = \frac{k_0^{1.5}}{l_\varepsilon}. \tag{16}$$

In the case T3A, the inlet flow velocity is 5 m/s and the free-stream turbulence intensity is 3%. The length of the plate is

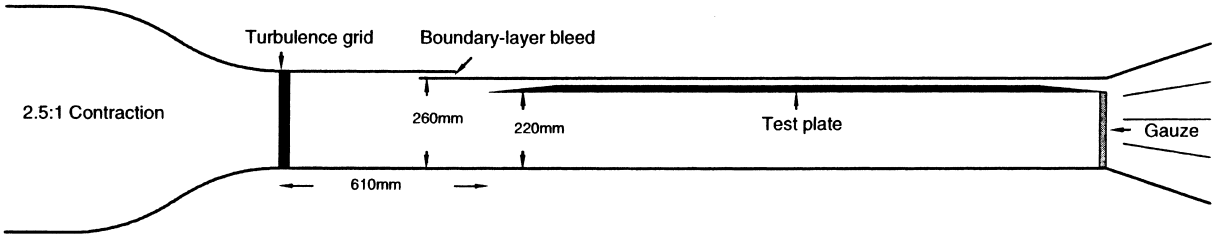

Fig. 1. The experimental setup for transitional flows over a sharp-leading-edge flat plate with zero pressure gradient.

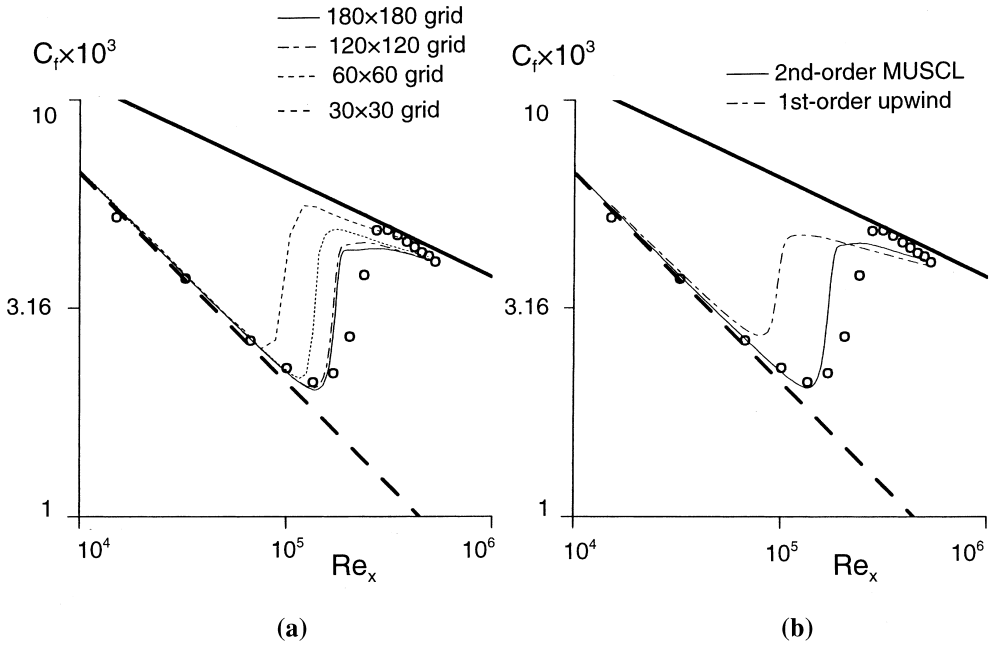

Fig. 2. Case T3A, skin-friction distributions predicted with the Launder–Sharma model with (a) four different grids and (b) two different convection schemes in k and ε equations.

1.6 m, and the Reynolds number based on the plate length, Re_L, is equal to 5.22×10^5. The computational domain extends to 0.15 m upstream of the leading-edge to facilitate an unambiguous specification of free-stream conditions. The thickness of the domain is 0.15 m, which is about five times larger than the boundary layer thickness at the end of the plate. Fig. 2(a) shows that a fine 120×120 grid is necessary here to achieve grid-independence with the linear model. In addition, as shown in Fig. 2(b), the use of a second-order scheme for approximating convection of k and ε is crucially important and yields major improvements in predictive realism, highlighting the extremely sensitive nature of transitional-flow computations and the importance of numerical accuracy. Thus, all computations to follow have been performed on the fine 120×120 grid using the second-order MUSCL scheme, applied to both momentum and turbulence quantities.

Although the use of the elliptic solver allows inlet velocity and turbulence intensity to be prescribed with a high degree of confidence, the dissipation-rate length scale, l_ε, is unknown and requires careful consideration. The specification of l_ε is guided by the measured free-stream turbulence-energy decay, and its value may be determined by observing what level of inlet value yields the correct decay rate. Computational experiments show that the use of $l_\varepsilon = 10$ mm yields the correct decay rate. This approach to prescribing the free-stream l_ε value is essential, and Rodi (1991), among others, has shown that l_ε can have a profound effect on the predicted transitional behaviour.

Predicted skin-friction distributions are shown in Fig. 3(a). It is observed that all models return similar positions for the onset of transition, the two-equation cubic model giving the closest agreement with the experimental data. However, this model also predicts an overshoot at the end of transition and underestimates the skin-friction in the fully turbulent region. The linear variant gives the earliest transition and also results in an insufficient level of skin friction after transition. The three-equation model, on the other hand, slightly overestimates the skin friction after transition, but returns the best result in terms of its magnitude and trend. Fig. 3(b) compares variations of shape-factor. Since the length of transition is not fully reproduced by any of the models, there are some expected and consistent discrepancies between the predictions and the data for the shape factor, especially within the transitional region.

Profiles of the three normal turbulence intensities at three representative streamwise positions are given in Fig. 4, the first position being within the 'laminar' (pre-transitional) portion. No results arising from the linear model have been included here as this model is obviously unable to predict realistic levels of normal-stress anisotropy. A comparison of Fig. 4(a) with Fig. 4(b) reveals the superiority of the three-equation model which returns more pronounced near-wall anisotropy for v' and w', in line with the experimental data, whilst the two-equation form predicts insufficient separation between the normal-intensity components. Neither model represents correctly the pre-transitional state which is characterized by a laminar-like mean-flow behaviour, and hence very low turbulent shear stress, but nonetheless a significant level of streamwise intensity.

4.2. Flow over a flat-plate with a sharp leading edge at variable pressure gradient

The principal objective of the T3C series of tests (Roach and Brierley, 1992) is to identify the ability of turbulence models to predict the effect of free-stream turbulence intensity and Reynolds number on the transitional behaviour of boundary layers in an initially favourable pressure gradient followed by an adverse pressure gradient, a condition representative of an aft-loaded turbine blade. There are five test cases in the T3C series, for which the inlet flow conditions are given in Table 3. The approach flows for T3C2–T3C5 have the same turbulence intensity of 3% but different mean velocities, whereas in T3C1 the turbulence intensity is 8%. Among the T3C test cases, T3C2 has exactly the same approach-flow conditions as those pertaining to T3A. This allows the effect of pressure gradient on transition to be examined in isolation, without the obscuring influence of variations in other properties. In what

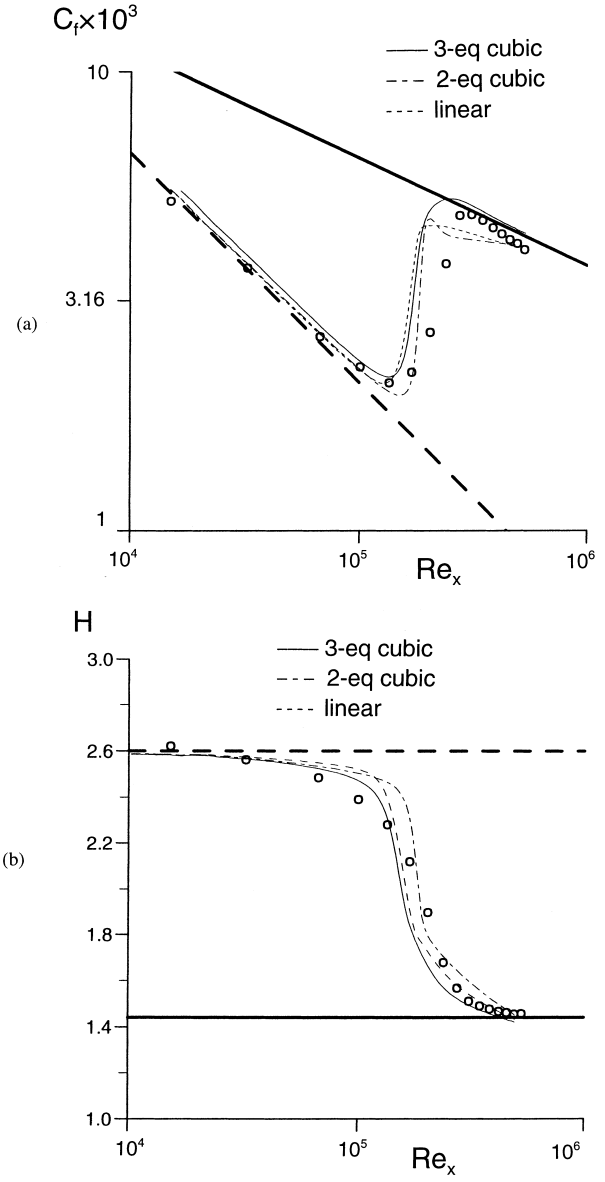

Fig. 3. Case T3A, distributions of (a) skin-friction and (b) shape factor.

follows, the cases presented are T3C1, T3C5 and T3C2. In the first two, transition occurs in the upstream acceleration region, while in the third case, transition is delayed and induced in the downstream deceleration region.

Rather than prescribing the velocity distribution along the free-stream boundary, as would have to be done with a parabolic boundary-layer algorithm, the approach adopted here computes the variable free-stream velocity as a natural consequence of the displacement effect arising from the channel bump. It is appropriate, therefore, to examine the agreement of the predicted free-stream velocity with the data. This is done in Fig. 5 which shows the distribution of the free-stream acceleration parameter, K, for case T3C1. As expected, excellent agreement with the measured data is returned by all models. It is also noted that K is very high near the leading edge, well above the value 3×10^{-6} normally associated with relaminarisation. In the presence of such a high level of acceleration, the initial decay of free-stream turbulence is enhanced. Fig. 6 shows the decay of free-stream turbulence for case T3C2, and this verifies that the choice of $l_\varepsilon = 8$ mm ($l_\varepsilon = 13.6$ mm for T3C1 and $l_\varepsilon = 9$ mm for T3C5) at inlet ensures close adherence to the experimental variation along the entire boundary layer.

Distributions of skin-friction and shape factor for cases T3C1, T3C5 and T3C2 are presented in Fig. 7. The bump that generates the streamwise pressure gradient is included in the figure to reveal the location of transition in relation to the bump crest. In T3C1 and T3C5, in which the inlet turbulence intensity or velocity is especially high, transition begins and ends in the favourable pressure-gradient region, and the transition process is prolonged as a consequence of the sustained acceleration. Although the models correctly predict transition to occur within the favourable pressure-gradient region, the length of the transition region is not very well returned. Among the models examined, both cubic forms yield fairly close agreement with the data in terms of the onset of transition. However, the skin-friction predicted by the two-equation version and by the linear form is again under-estimated following transition. The three-equation variant gives better agreement with the data in terms of the magnitude of skin-friction after transition. It is also noted that the rapid drop in skin-friction in the decelerating, adverse-pressure-gradient region is well captured by this model. In comparison with T3C1, the inlet velocity and turbulence intensity for case T3C2 are both lower, and the transition region has now shifted downstream to the adverse-pressure-gradient portion. The experiment suggests that the length of transition is significantly shortened, relative to the previous cases, under the influence of the adverse pressure gradient. The two-equation cubic model yields the best prediction in terms of the onset of transition, but the length of transition continues to be under-estimated. The three-equation and the linear models seriously misrepresent the onset of transition, in marked contrast to the previous cases.

Profiles of mean velocity and turbulence intensity of T3C1 at three representative streamwise positions are presented in Fig. 8. All models predict velocity fields which are in fair agreement with the experimental data. Fig. 8(b) indicates that the three-equation model again gives the best results for the streamwise turbulence intensity. However, within the downstream deceleration region ($Re_x = 7.8 \times 10^5$), the model over-estimates the near-wall value, implying that the near-wall turbulence energy is excessive in the deceleration region.

In all three models investigated herein, the dependence of the damping function f_μ on R_t is an important factor in their predictive performance. On physical grounds, this dependence should be confined to $0 < y^+ < 20$. Beyond this layer, the damping of turbulence (and the shear stress) is effected, principally, by the inviscid process of a pressure-reflection-induced preferential reduction of the wall-normal intensity v', which then gives rise to a rapid increase in turbulence anisotropy as the wall is approached. This is the physical reason underlying the use of A_2 as a parameter in c_μ in the three-equation variant. The two-equation form, in contrast, attempts to represent this process via strain and vorticity invariants, while the linear form relies entirely on f_μ to achieve the requisite damping. The combined damping effect of $c_\mu f_\mu$ in equilibrium conditions predicted by the present models is shown in Fig. 9 relative to experimental data. These results have been taken from Suga (1995). In contrast, the fragment responsible purely for viscosity-induced damping is shown in Fig. 10. As seen, both the linear and the two-equation cubic models rely inappropriately heavily on R_t-induced damping, while this dependence is perhaps too weak in the three-equation form, extending only to $y^+ = 6$. Increasing this dependence can be achieved, for example, by decreasing the numerical factor multiplying R_t in c_μ. The effect of (arbitrarily) reducing the factor 1/30 to 1/40 in

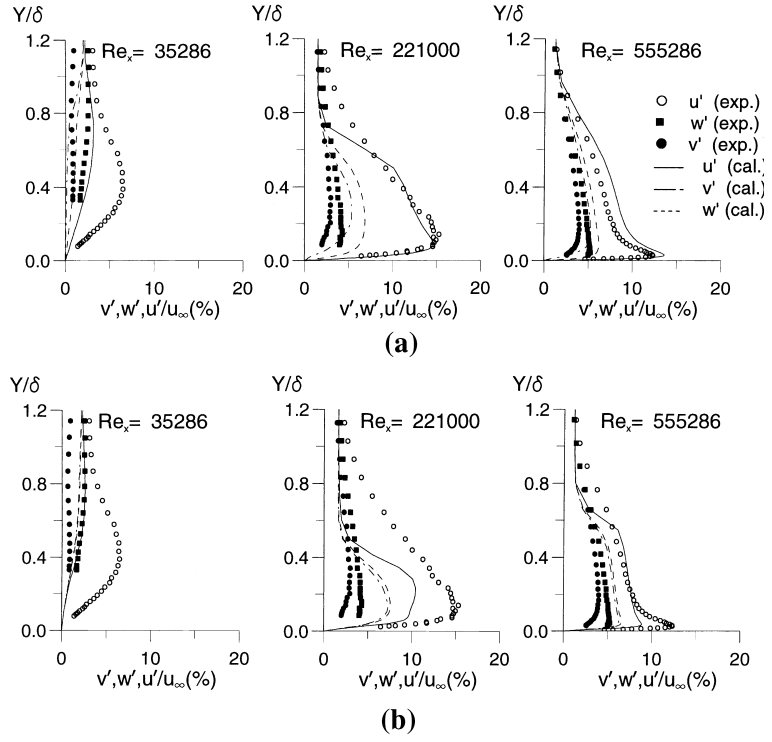

Fig. 4. Case T3A, turbulence-intensity profiles, (a) three-equation cubic model and (b) two-equation cubic model.

Table 3
Inlet flow conditions for all T3C test cases

Test case	T3C1	T3C2	T3C3	T3C4	T3C5
Tu_0 (%)	8	3	3	3	3
u_0 (m/s)	6.2	5.0	4.2	1.36	9.2

the f_μ function (8) is shown in Fig. 11 to result in a significant downstream shift in the transition location. While this is desirable, it must be noted that the modification leads, without changes to the dependence on A_2, to a deterioration in the behaviour of $c_\mu f_\mu$ (Fig. 9). Hence a general improvement in model performance in variable pressure gradient requires a comprehensive exercise by reference to equilibrium as well as non-equilibrium flows.

5. Conclusions

The transitional flows examined in this paper form a basic set of test cases, allowing a searching investigation of model performance to be undertaken for fundamentally important flow conditions. The computations performed allow the following conclusions to be drawn:

1. For the simplest test case, T3A, the three-equation non-linear model returns the best performance, especially in the fully turbulent region where the model gives excellent agreement with the experimental data. In the 'laminar' (pre-tran-

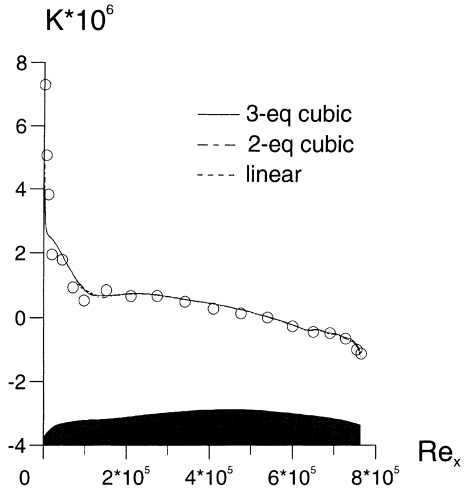

Fig. 5. Case T3C1, distributions of free-stream acceleration parameter.

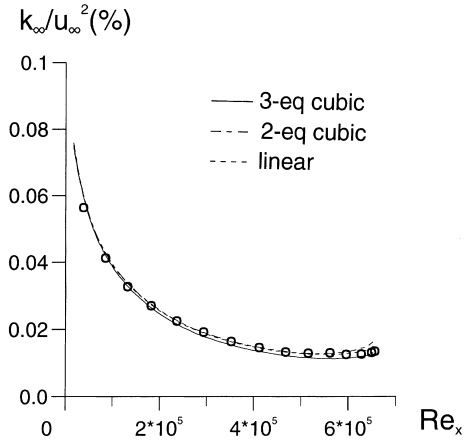

Fig. 6. Case T3C2, free-stream turbulence decay.

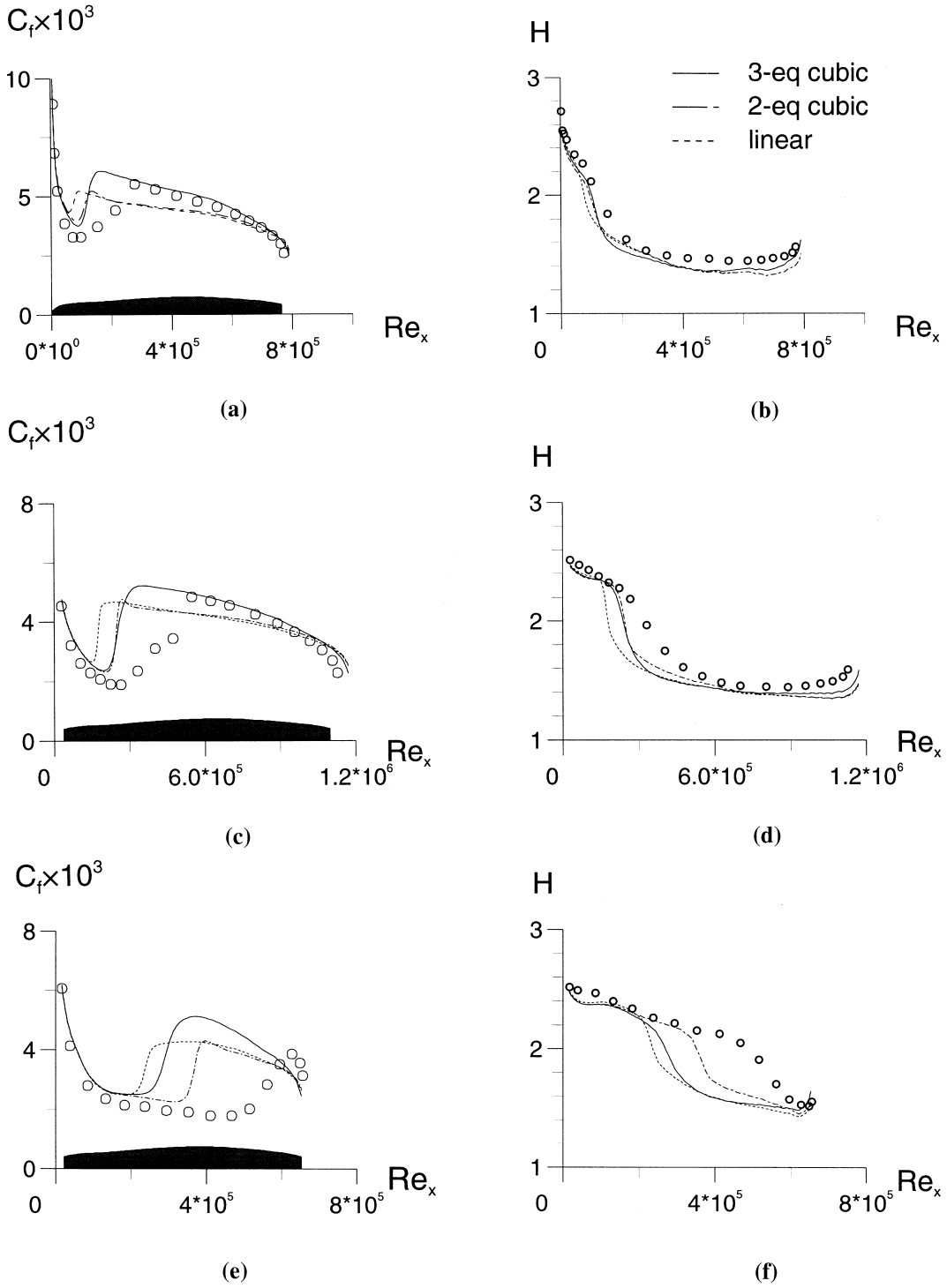

Fig. 7. Cases T3C1, T3C5 and T3C2, distributions of (a) T3C1, skin-friction, (b) T3C1, shape factor, (c) T3C5, skin-friction, (d) T3C5, shape factor, (e) T3C2, skin-friction and (f) T3C2, shape factor.

sitional) region, however, the model's performance is rather poor. Although this model slightly over-estimates the skin-friction in the turbulent regime – a defect rooted in a somewhat excessive level of shear stress – the position and trend of transition and the magnitude of skin-friction are generally well represented.

2. In the more challenging T3C test cases, all models under-estimate the length of transition, especially when transition occurs in the favourable-pressure-gradient portion of the flow, in which case the experimentally observed transition length is drawn out.
3. Although the dependence of the models on R_t, through the f_μ function, may not reflect correctly the actual physics of the flow, its inclusion is important and can affect the quality of the predictions, especially the onset of transition. This applies in particular when the Reynolds number is low.

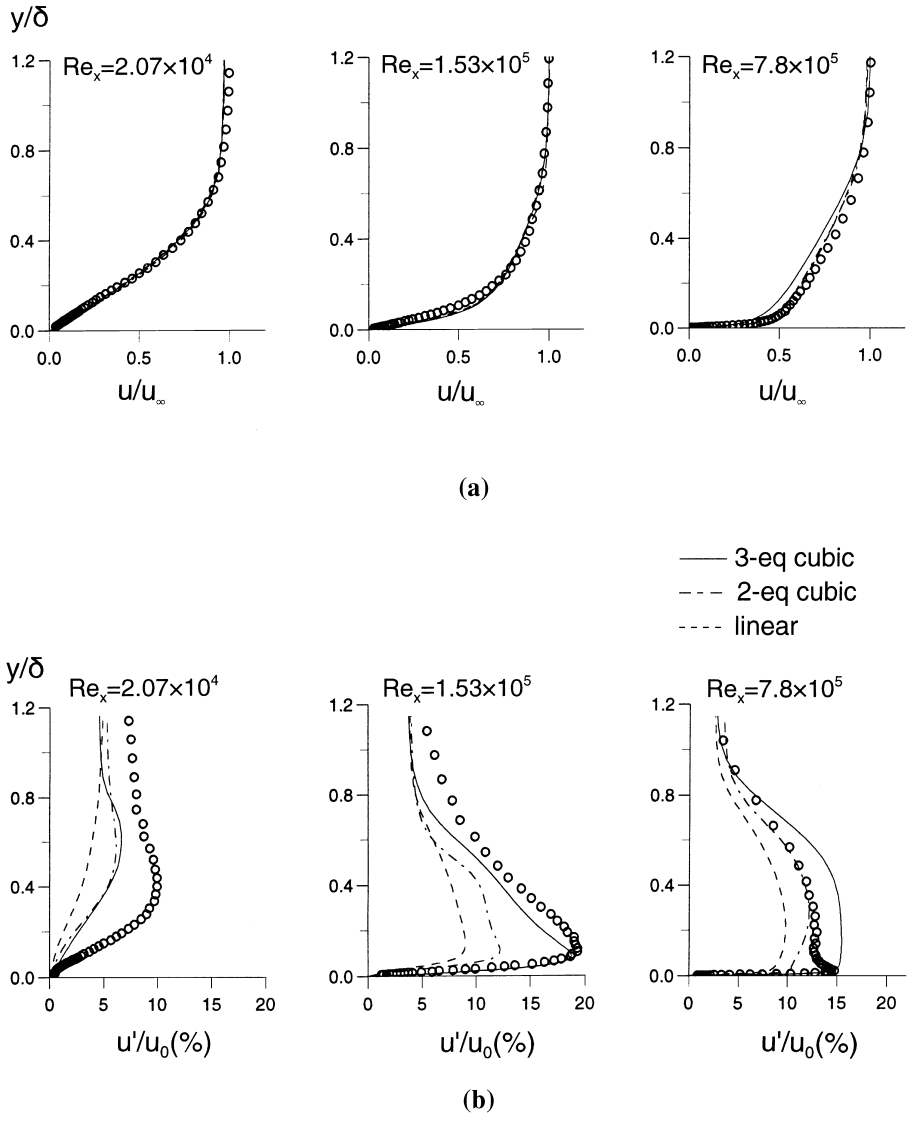

Fig. 8. Case T3C1, distributions of (a) streamwise mean-velocity profiles and (b) streamwise turbulence-intensity profiles.

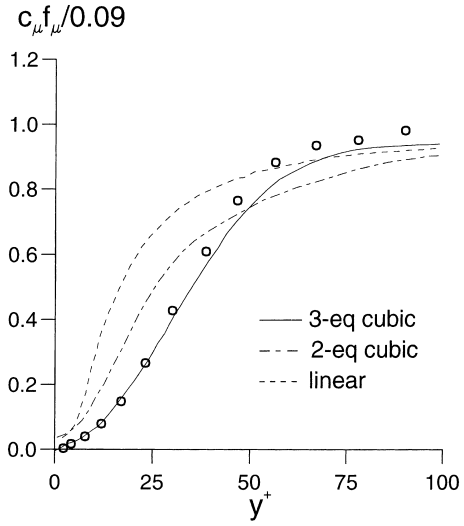

Fig. 9. Distributions of $c_\mu f_\mu/0.09$ predicted by different models in fully developed channel flow at Re = 5400 (results from Suga, 1995).

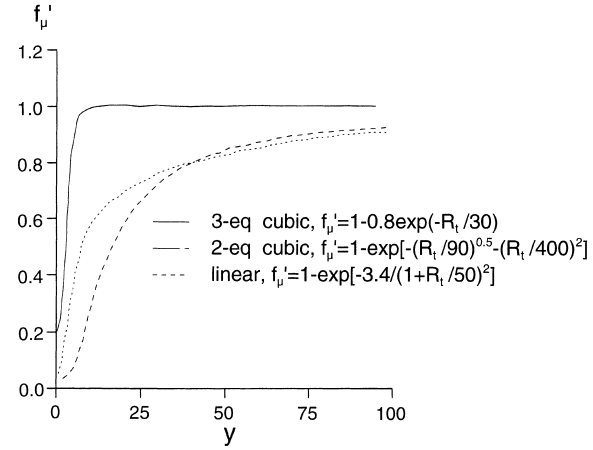

Fig. 10. Dependence of f'_μ on R_t predicted by different models in fully developed channel at Re = 5400 (results from Suga, 1995).

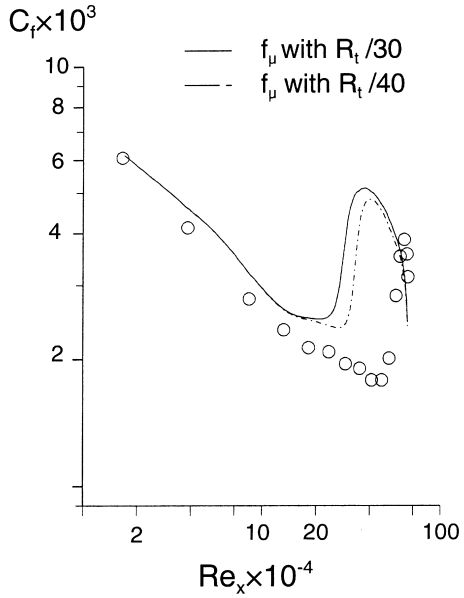

Fig. 11. Case T3C2, skin-friction distributions predicted by three-equation cubic model with different coefficients used in the f_μ function.

4. The computations for the T3C cases indicate that the two-equation non-linear model gives, overall, the best predictions in terms of the onset of transition, particularly when the Reynolds number is low, whilst the three-equation form yields the closest agreement with data for normal stresses. The performance of the latter can be improved by significantly strengthening the R_t-dependence in the f_μ function. However, such a modification, apart from being questionable on physical grounds, requires changes in other parts of the model in compensation.

References

Abu-Ghannam, B.J., Shaw, R., 1980. Natural transition of boundary layers – The effects of turbulence, pressure gradient and flow history. J. Mech. Engrg. Sci. 22, 213.

Blair, M.F., 1983. Influence of free-stream turbulence on turbulent boundary layer heat transfer and mean profile development, Part I – Experimental Data. ASME J. Heat Transfer 105, 33.

Chen, W.L., 1996. Turbulence modelling for highly-loaded cascade blades. Ph.D. Thesis, UMIST, Manchester, UK.

Chen, W.L., Leschziner, M.A., Lien, F.S., 1998. Computational prediction of flow around highly-loaded compressor-cascade blades with non-linear eddy-viscosity models. Internat. J. Heat and Fluid Flow 19, 307.

Craft, T.J., Launder, B.E., Suga, K., 1993. Extending the applicability of eddy-viscosity model through the use of deformation invariant and non-linear elements. Proceedings of the Fifth International Symposium on Refined Flow Modelling and Turbulence Measurements, p. 125.

Craft, T.J., Launder, B.E., Suga, K., 1997. Prediction of turbulent transitional phenomena with a nonlinear eddy-viscosity model. Internat. J. Heat and Fluid Flow 18, 15.

Emmons, H.W., 1951. The laminar-turbulent transition in boundary layer – Part I. J. Aero. Sci. 18, 490.

Kim, J., Moin, P., Moser, R., 1987. Turbulence statistics in fully developed channel flow at low Reynolds number. J. Fluid Mech. 177, 133.

Launder, B.E., Sharma, B.I., 1974. Application of the energy-dissipation model of turbulence to the calculation of flow near a spinning disc. Internat. J. Heat Mass Transfer 1, 131.

Leonard, B.P., 1979. A stable and accurate convective modelling procedure based on quadratic upstream interpolation. Comput. Methods Appl. Mech. Engrg. 19, 59.

Lien, F.S., Leschziner, M.A., 1994a. A general non-orthogonal collocated FV algorithm for turbulent flow at all speed incorporating second-moment closure. Part 1: Computational implementation. Comput. Methods Appl. Mech. Engrg. 114, 123.

Lien, F.S., Leschziner, M.A., 1994b. A general non-orthogonal collocated FV algorithm for turbulent flow at all speed incorporating second-moment closure. Part 2: Application. Comput. Methods Appl. Mech. Engrg. 114, 149.

Mayle, R.E., 1991. The role of laminar-turbulent transition in gas turbine engines. ASME J. Turbomachinery 113, 509.

Roach, P.E., Brierley, D.H., 1992. Test Case T3A, T3B. Numerical Simulation of Unsteady and Transition to Turbulence. Cambridge University Press, Cambridge, p. 319.

Rodi, W., 1991. Experience with two-layer models combining the k-ε model with a one-equation model near the wall. AIAA Paper 91-0216.

Savill, A.M., 1991. Turbulence model predictions for transition under free-stream turbulence. Progress Report Poster Paper at RAeS Transition and Boundary Layer Control Conference. Cambridge.

Savill, A.M., 1995a. A summary report on the COST ERCOAFTAC transition SIG project evaluating turbulence models for predicting transition. ERCOFTAC Bulletin 24, 57.

Savill, A.M., 1995b. The SLY RST intermittency model for predicting transition. ERCOFTAC Bulletin 24, 37.

Steelant, J., Dick, E., 1994. Modelling of by-pass transition with conditioned Navier–Stokes equations and a k-ε model adapted for intermittency. ASME Paper 94-GT-12.

Suga, K., 1995. Development and application of a non-linear eddy viscosity model sensitized to stress and strain invariant. Ph.D. Thesis, UMIST, Manchester, UK.

van Leer, B., 1979. Towards the ultimate convection diffusion scheme V, a second-order sequel to Godunov's method. J. Comput. Phys. 32, 101.

Yang, Z., Voke, P.R., Savill, A.M., 1994. Mechanisms and models of boundary layer respectively deduced from large eddy simulation of bypass transition. In: Voke, P.R., Kleiser, L., Chollet, J.-P. (Eds.), Direct and Large Eddy Simulations 1. Kluwer Academic Publishers, pp. 225–236.

Yap, C.R., 1987. Turbulent heat and momentum transfer in recirculating and impinging flows, Ph.D. Thesis, UMIST, Manchester, UK.